



Published in final edited form as:

J Immunol. 2013 April 1; 190(7): 3197–3206. doi:10.4049/jimmunol.1202212.

Orai1 Function is Essential for T Cell Homing to Lymph Nodes

Milton L. Greenberg^{*,†,‡}, Ying Yu^{*,†,‡,1}, Sabrina Leverrier^{†,‡}, Shenyan L. Zhang^{†,‡,2}, Ian Parker^{†,§}, and Michael D. Cahalan^{†,‡}

[†] Department of Physiology and Biophysics, University of California, Irvine, CA

[‡] Institute for Immunology, University of California, Irvine, CA

[§] Department of Neurobiology and Behavior, University of California, Irvine, CA

Abstract

In T lymphocytes, Ca²⁺ release-activated Ca²⁺ (CRAC) channels composed of Orai1 subunits trigger antigen-induced gene expression and cell proliferation through the NFAT pathway. We evaluated the requirement of CRAC channel function for lymphocyte homing using expression of a dominant-negative Orai1-E106A mutant to suppress Ca²⁺ signaling. To investigate homing and motility of human lymphocytes in immunocompromised mouse hosts, we transferred human lymphocytes either acutely or following stable engraftment after a second transfer from the same blood donor. Human and mouse lymphocyte homing was assessed and cells were tracked within lymph nodes by two-photon microscopy. Our results demonstrate that human T and B lymphocytes home into and migrate within the lymph nodes of immunocompromised NOD.SCID mice similar to murine lymphocytes. Human T and B cells colocalized in atrophied or reconstituted mouse lymph nodes, where T cells migrated in a random walk at velocities of 9–13 $\mu\text{m}/\text{min}$ and B cells at 6 $\mu\text{m}/\text{min}$. Expression of Orai1-E106A inhibited CRAC channel function in human and mouse T cells and prevented homing from high endothelial venules into murine lymph nodes. Ca²⁺ signals induced by CCL21 were also inhibited in T cells expressing Orai1-E106A. With CRAC channels inhibited, the high-affinity form of LFA-1 failed to become active, and T cells failed to migrate across endothelial cells in a transwell model. These results establish a requirement for CRAC channel-mediated Ca²⁺ influx for T cell homing to lymph nodes mediated by high-affinity integrin activation and chemokine-induced transendothelial migration.

Introduction

Sustained Ca²⁺ influx through Ca²⁺ release-activated Ca²⁺ (CRAC) channels is essential for antigen-dependent T cell activation and proliferation via NFAT-driven gene expression (1, 2). In addition, following T cell receptor engagement, CRAC channel activation elevates cytosolic calcium ([Ca²⁺]_i) and acts to halt T cell migration and facilitate prolonged interactions with antigen presenting cells (3). RNA interference screening and mutagenesis have identified two proteins that activate and form the CRAC channel: STIM proteins (STIM1 and STIM2 in mammals) as the ER-resident Ca²⁺ sensor; and Orai proteins (Orai1, Orai2, and Orai3 in humans) as the Ca²⁺-selective pore-forming subunit (4–9). In T cells and other cells of the immune system, Ca²⁺ store depletion induces STIM1 to migrate as oligomers from the bulk ER to junctions immediately adjacent to the plasma membrane and mediates Ca²⁺ influx by opening Orai1 channels by direct STIM1-Orai1 interaction (10).

Address correspondence to Dr. Michael D. Cahalan, Department of Physiology and Biophysics, University of California, Irvine CA 92697, mcahalan@uci.edu, phone: (949) 824-7776, fax: (949) 824-3143.

*These authors contributed equally to this study.

¹Present address: Alcon laboratories Inc. Fort Worth, TX.

²Present address: Department of Systems Biology and Translational Medicine, Texas A&M Health Science Center, Temple, TX.

Although the properties of CRAC channels and their role in T cell Ca^{2+} signaling have been described in detail (11, 12), the functional roles of CRAC channels in human T cell activation and immune defense remain incompletely characterized. In particular, CRAC channels may also be required for lymphocyte trafficking and migration. To address this, we developed methods to engraft and visualize human lymphocytes in the context of immunocompromised mouse models, and expressed a dominant-inhibitory Orai1 construct to evaluate the functional role of CRAC channel activity in lymphocyte homing to lymph nodes *in vivo*.

Several mutations in Orai1 or STIM1 have been identified in human patients with severe combined immune deficiency (SCID), leading to inhibition of CRAC channel function and lethal immune suppression (7, 13-16). In patients with the homozygous Orai1-R91W mutation, CRAC channels fail to open, and T cells cannot take up Ca^{2+} following stimulation (7). In contrast, Ca^{2+} influx in T cells isolated from Orai1-deficient mice was only partially inhibited (17, 18), perhaps due to compensation by other Orai isoforms. We therefore sought an alternative method to evaluate CRAC channel function. A charge-neutralizing mutation of the critical glutamate residue to alanine in *Drosophila* Orai or human Orai1 has a dominant-negative effect on the CRAC channel, resulting in a non-conducting channel (4, 5). In this study, we use expression of the dominant-negative Orai1-E106A to silence the CRAC channel and inhibit Ca^{2+} influx so as to evaluate the functional role for Orai1 in homing.

T cell homing from the blood into secondary lymphoid organs (SLO) occurs by migration across the high endothelial venules (HEV) and is required for adaptive immunity. This process is sequentially mediated by selectins, including CD62L, that facilitate tethering, cellular adhesion, and rolling within the HEV lumen (19); and chemokines and chemokine receptors that activate integrins and direct migration from the venules (20, 21). The chemokine receptor CCR7 and its ligands CCL19 and CCL21 play a significant role in T cell homing and facilitate activation of the β_2 integrin complex LFA-1, which allows interactions with intercellular adhesion molecule 1 (ICAM-1) on the surface of the endothelium (22, 23). Elevations in $[\text{Ca}^{2+}]_i$ have been shown to activate LFA-1 and induce lateral clustering on the T cell surface (24). CCL21 treatment induces Ca^{2+} influx in human T cells (25, 26), but it is unknown if CCL21-induced Ca^{2+} signaling through Orai1 channels facilitates integrin activation and homing into lymph nodes (LN).

Two-photon microscopy enables real-time visualization of immune cell migration and dynamics within the SLO of mice (27). However, it is not feasible to directly manipulate and image human immune cells in a native *in vivo* environment. Therefore, we sought an *in vivo* system using an immunocompromised murine host to visualize human T cell motility. Non-obese diabetic/severe combined immunodeficiency (NOD.SCID) mice are characterized by defects in innate and adaptive immunity, including atrophied lymph nodes devoid of T and B lymphocytes and reduced natural killer cell activity (28). Several NOD.SCID strains have been validated as recipients for reconstitution with human hematopoietic cells and are useful for establishing durable human xenografts (29-31). In this study, we first established human lymphocyte xenografted models for two-photon imaging of human cells in an *in vivo* environment, and characterized the motility of human T and B lymphocytes in comparison with murine cells in the immunocompromised murine host LNs. We utilized both the original NOD.SCID strain and NOD.SCID.B2 mice with β_2 microglobulin knocked out. The latter strain lacks lymphoid and NK cells and has been shown to permit enhanced engraftment of human T cells (32). We then utilized this model system to in conjunction with expression of the dominant-negative Orai1-E106A mutant to investigate the role of Ca^{2+} influx through CRAC channels for integrin activation, chemokine responses, and homing of human and murine T cells.

Materials and Methods

Mice

NOD.CB17-Prkdc^{scid}/J (NOD.SCID) mice obtained from Jackson Laboratory (Bar Harbor, ME, USA, Stock # 001303) were housed and monitored in a specific pathogen-free environment with sterile food and water in our animal facility. To inhibit NK cell activity, NOD.SCID mice were i.v. injected with 20 μ L anti-NK cell antibody (rabbit anti-Asialo GM1, Wako Bioproducts, Richmond, VA) according to manufacturer's instructions 3-4 days before adoptive transfer of human T cells. NOD.Cg-Prkdc^{scid} B2m^{tm1Unc}/J mice (NOD.SCID.B2) and C57.BL/6J mice were obtained from Jackson Laboratory (Stock #002570, #000664). Mice used were between 8 and 18 weeks of age. NOD.SCID.B2 mice were reconstituted with human peripheral blood leukocytes (PBLs) as described (30). 3×10^7 human PBL were injected intraperitoneally and experiments were performed three weeks later. All of the experimental procedures were approved by the Animal Care and Use Committee of University of California, Irvine.

Purification of human monocytes and isolation of CD4⁺, CD8⁺, CD19⁺ and CD3⁺ cells

Human PBLs were isolated from blood of voluntary healthy donors by Ficoll-Hypaque (gradient=1.077 g/dl) density gradient centrifugation. Isolation of human CD4⁺ and CD8⁺ T cells was performed using human CD4⁺ and CD8⁺ T cell isolation kits (Miltenyi Biotec, Bergish Gladbach, Germany) according to manufacturer's instructions. To prepare human CD8⁺ T cells, PBLs were first suspended in labeling buffer and incubated with anti-CD8 mAb-coated microbeads. CD8⁺ T cells were isolated by positive selection using a magnetic cell separation system (MACS; Miltenyi Biotec). To prepare human CD4⁺ T cells, the remaining cells were isolated by negative selection with a CD4⁺ T cell isolation cocktail. CD19⁺ B cells were isolated by positive selection according to manufacturer's instructions (Miltenyi Biotec). In some experiments, human CD3⁺ T cells were isolated using EasySep Human CD3⁺ Isolation kit (StemCell Technologies, Vancouver, BC, Canada) according to manufacturer's instructions. The purity of CD4⁺, CD8⁺, CD19⁺ or CD3⁺ cell populations was confirmed to be >95% by flow cytometry.

Cell adoptive transfer in mice

For human T cells, purified CD4⁺ and CD8⁺ T cells and CD19⁺ B cells were separately labeled with CellTracker dyes (Invitrogen, Grand Island, NY) 5-(and-6)-carboxyfluorescein diacetate succinimidyl ester (CFSE, 4 μ M), 5-(and-6)-(((4-chloromethyl)benzoyl) amino) tetramethylrhodamine (CMTMR, 8 μ M) or 4-chloromethyl-6,8-difluoro-7-hydroxycoumarin (CMF₂HC, 20 μ M) for 10-60 min at 37°C and adoptively transferred into NOD.SCID mice. For comparison, mouse CD4⁺ T cells were isolated from lymph nodes of wildtype C57.BL/6J mice by magnetic negative selection (Miltenyi Biotec), labeled with CFSE and transferred into NOD.SCID mice. CD3⁺ human T cells were labeled with CMTMR and transferred into reconstituted NOD.SCID.B2 mice. For all adoptive transfer experiments, 5×10^6 labeled cells of each cell type were transferred by tail-vein or retro-orbital injection.

Transfection and retroviral transduction

Primary human T cells were transfected by nucleofection (Amaxa, Allendale, NJ), using the high-viability protocol with enhanced green fluorescent protein (eGFP), eGFP-tagged Orail-E106A mutant, or mock transfected with no plasmid as indicated. Human cells were used for experiments 24 hr after transfection. Constructs were generated as described previously (33). Retroviral transduction of purified mouse T cells was performed as described (34). Thy1.1-CFP or Thy1.1-eGFP-Orail-E106A retroviral vectors were transfected into 293T

cells and retroviral supernatant was collected. Activated primary mouse T cells were spin-fected using retroviral supernatant and 4 $\mu\text{g/ml}$ polybrene (Sigma-Aldrich, St. Louis, MO) for 1 hr at 1800 rpm, and incubated for 24–48 hr at 37°C. Transduced mouse T cells expressing the retrovirus (Thy1.1⁺) were magnetically isolated from non-expressing cells (Thy1.1⁻) using a biotinylated anti-Thy1.1 antibody according to manufacturer's instructions (Miltenyi Biotech). Following purification, Thy1.1⁻CFP⁻ cells were labeled with CMTMR and Thy1.1⁻eGFP-Orai1-E106A⁻ cells were labeled with CFSE. Also, Thy1.1⁺CFP⁺ were labeled with CMTMR and Thy1.1⁺eGFP-Orai1-E106A⁺ were labeled with CFSE. For determination of homing efficiency, fluorescently labeled Thy1.1⁻ or Thy1.1⁺ populations were co-adoptively transferred into wildtype C57.B16 recipient mice.

Two-photon imaging and analysis

Multi-dimensional (x, y, z, time, emission wavelength) two-photon microscopy was employed to image fluorescently labeled lymphocytes in explanted mouse lymph nodes, using a 780 nm femtosecond pulsed laser as described previously (35). Fluorescence emission was split by 510 nm & 560 nm dichroic mirrors into three detector channels, used to visualize CFSE-labeled (green), CMTMR-labeled (red) and CMF₂HC-labeled (blue) adoptively-transferred cells. To image the lymph nodes, tissue was oriented with the hilum away from the dipping objective (Olympus 20x, NA 0.9) of the upright microscope. The node was maintained at 36–37°C by perfusion with medium (RPMI) bubbled with carbogen (95% O₂ / 5% CO₂). 3D image stacks were sequentially acquired and the x,y,z coordinates of individual lymphocytes in the intact lymphoid organ were used to create individual cell tracks. Imaging volumes of x=200 μm , y=162 μm , and z=50 μm were acquired at 18–20 second intervals using MetaMorph software (Universal Imaging, Sunnyvale, CA). This volume collection was repeated for up to 40 min to create a 4D data set. Data were processed and analyzed using Imaris software (Bitplane, South Windsor, CT). To reduce selection bias in our analysis of motility and trajectory, all clearly visible cells were tracked from each video segment.

Immunohistochemistry

LN specimens were fixed in 4% neutrally buffered formaldehyde. 5–6 μm thick paraffin-embedded serial tissue sections were mounted on positively-charged glass slides. Sections were taken for hematoxylin and eosin (H&E) staining or immunofluorescence staining. Sections were bathed in xylene then treated with a graded series of alcohol [100, 95, and 75% ethanol (v/v) H₂O] and rehydrated in PBS (pH 7.5). Sections were treated with Retrieval A (pH 6.0, BD) and microwaved for 10 min for antigen retrieval. Sections were incubated with 3% H₂O₂ in PBS to block endogenous peroxidase activity for 10 min followed by incubation with blocking solution containing 1% normal goat serum for 20 min. Samples were then stained with anti-PNAd mAb MECA-79 (1:20 dilution, Rat IgM; BD) overnight at 4°C. Secondary detection antibodies were Cy5-conjugated goat anti-rat IgM +IgG (Jackson Laboratories). Slides were analyzed by fluorescence microscopy using a Zeiss Axioskop microscope (Carl Zeiss, Thornwood, NY).

Flow cytometry

Cells were analyzed using FACSCalibur flow cytometer with CellQuest software or a LSRII with FACSDiva software (Becton Dickinson, Mountain View, CA). Anti-human CD45, CD4, CD8, CCR7, and CD62L and the corresponding isotype control antibodies were obtained from eBioscience (San Diego, CA). Conformation-specific Abs against human LFA-1 (MEM-83) and VLA-4 (12G10) were purchased from Abcam (Cambridge, MA). TRITC-conjugated secondary Abs were purchased from KPL (Gaithersburg, Maryland). Annexin V-PE was purchased from BD. Cells were suspended in buffer containing 0.5% BSA and 2 mM EDTA in PBS (staining buffer) and stained for 20–30 min with specific PE-

Cy5-conjugated mAbs. Unbound Abs were removed by two washes with staining buffer, and cells were resuspended in staining buffer and analyzed. For homing experiments, mouse lymph nodes and spleen were collected 18 hr following adoptive transfer and made into single-cell suspensions with 70 μm nylon cell strainers (BD Falcon, Mountain View, CA). Cells were gated for appropriate forward and side scatter. Data were saved as FCS 2.0 list mode files and analyzed with FCS Express 1.3 or FlowJo.

Single-cell Ca^{2+} imaging and intracellular Ca^{2+} measurement by flow cytometry

Ratiometric single-cell Ca^{2+} imaging was performed as described (36). Cells were loaded by incubation for 30 min with 3 μM fura-2AM (Invitrogen) and analyzed following 2 μM thapsigargin (Tg; Sigma-Aldrich) treatment. Data were analyzed with Metafluor software (Universal Imaging) and Origin software (OriginLab, Northampton, MA). For flow cytometry, cells were analyzed on a BD LSR II flow cytometer with FACSDiva software (BD). eGFP- or eGFP-Orai1-E106A-transfected $\text{CD}3^+$ human T cells were loaded by incubation for 30 min with 8 μM fura red, AM (Invitrogen) at 37°C for 30 min, washed once and resuspended in 2 mM Ca^{2+} RPMI-1640 supplemented with 1% FCS at 5×10^5 cells/ml. An 800 μl aliquot was warmed to 37°C prior to stimulation. Cells were maintained at 37°C and analyzed at 500 events per second. After establishment of the baseline, the tube containing the cells was removed, stimulant was added, and the tube was replaced. Recording was continued for up to 200 s. Data were saved as FCS 2.0 list mode files and analyzed with the Flowjo Kinetics tool. $[\text{Ca}^{2+}]_i$ was determined as described previously (37).

Chemokines and transwell assays

Chemokines were obtained from PeproTech (Rocky Hill, NJ) and prepared according to manufacturer's instructions. Transwell assay plates with 5- μm pore size were obtained from Corning (Tewksbury, MA). HUVEC (human umbilical vein endothelial cells) were isolated as described previously (38). HUVECS were plated in M199 (Invitrogen) supplemented with 10% FCS and endothelial cell supplement (BD) on 1% gelatin coated inverted transwells and allowed to proliferate to confluency. HUVECs and transfected human T lymphocytes were plated in M199 (Invitrogen) supplemented with 10% FCS. The percentage migrated after 3 hr was calculated as a percentage of the total input. Chemotaxis assays were performed in triplicate with multiple donors for each cell type.

Soluble ICAM-1 Binding Assay

Transfected human $\text{CD}3^+$ T cells were suspended in 2 mM Ca^{2+} RPMI-1640 supplemented with 1% FCS. Cells were treated with 100 ng/ml rmCCL21 in the presence of ICAM-1/Fc (20 $\mu\text{g/ml}$; R&D Systems) and allophycocyanin-conjugated anti-human IgG1 (Fc-specific; Southern Biotechnology) for 10 min at 37°C. Change in ICAM-1 binding determined by flow cytometry was measured as a fold increase over control.

Statistical analysis

Statistical significance was determined using the student *t* test. Two-way analysis of covariance (ANCOVA) was used where indicated and was calculated using R Statistical Computing Software (Vienna, Austria). A value of $p < 0.05$ was considered significant. Data are presented as mean \pm SEM.

Results

Live-cell imaging of human lymphocytes in immunocompromised mice

To establish a system for *in vivo* imaging of human lymphocytes, we initially transferred human lymphocytes into NOD.SCID mice by intravenous injection (Supplemental Fig. 1A). Purified CD4⁺ and CD8⁺ T cells and CD19⁺ B cells distributed randomly throughout the atrophied LN, not localizing into any compartmentalized structure (Supplemental Fig. 2A, 2B, 2C), and actively migrated in a stop-and-go pattern of motility (Fig. 1A, Supplemental Video 1). Human CD4⁺ T cells migrated with a mean velocity of $9.3 \pm 0.4 \mu\text{m min}^{-1}$ (Fig. 1B). For comparison, adoptively transferred wildtype mouse CD4⁺ T cells also distributed randomly throughout the LN of NOD.SCID mice (Supplemental Fig. 2D) and migrated with slightly higher mean velocities averaging $10.9 \pm 0.2 \mu\text{m min}^{-1}$ (Supplemental Fig. 2E). Migrating human CD4⁺ T cells traversed a wide area, and their displacement from the origin increased in proportion to the square root of time (Fig. 1C, 1D). These properties are consistent with a default random-walk pattern of motility of human T cells in the immunocompromised mouse host. Analysis of turning angles between consecutive imaging frames revealed a mean turning angle of 69 ± 4.5 degrees (Fig 1E). Human CD8⁺ T cells performed similarly to human CD4⁺ cells, migrating with a mean velocity of $9.7 \pm 0.4 \mu\text{m min}^{-1}$ (Fig. 1F), with displacement increasing as a square root function of time (Fig. 1G, 1H) and with a similar mean turning angle (Fig. 1I). Human CD19⁺ B cells co-localized with and migrated more slowly than CD4⁺ or CD8⁺ T cells, with a mean velocity of $5.8 \pm 0.3 \mu\text{m min}^{-1}$ (Fig. 1J), displacing about half the distance of human T cells (Fig. 1K, 1L), and along more tortuous paths with a mean turning angle of 94 ± 4.8 degrees (Fig. 1M). This analysis of human lymphocyte motility is in agreement with previous two-photon imaging, which showed that murine T cells migrate faster and along straighter paths than B cells (39). We conclude that human T and B cells migrate similarly to mouse T and B cells in the host lymph node environment, with velocities that are only slightly slower than mouse cells. Despite the lack of organization into separate T zones and follicles, both human and mouse T cells migrated faster than co-localized B cells, implying an intrinsically faster mechanism for crawling.

Functional CRAC channels are required for human T cell homing in NOD.SCID mice

The human xenograft model provides an opportunity to observe human lymphocytes that have been manipulated by transfection prior to adoptive transfer. Purified human CD4⁺ T cells were transfected with control eGFP or with the dominant-negative eGFP-Orai1-E106A CRAC channel mutant and rested overnight in culture. Expression of eGFP-Orai1-E106A had no effect on cell viability prior to transfer as determined by Annexin V staining, an indicator of apoptosis (Supplemental Fig. 3A). Aliquots of cells were evaluated by flow cytometry, revealing a transfection efficiency of >50% (Fig. 2A). Ca²⁺ imaging confirmed that, as expected, human T cells expressing eGFP-Orai1-E106A showed impaired Ca²⁺ influx following re-addition of external Ca²⁺ after Tg treatment to deplete ER Ca²⁺ stores (Fig. 2B). To quantify human T cell homing to the SLO in the xenograft model, T cells were transferred into a NOD.SCID recipient and analyzed by flow cytometry (Supplemental Fig. 1B). Control eGFP⁺ human T cells efficiently homed to both the LNs and spleen. In contrast, eGFP-Orai1-E106A⁺ human T cells were almost entirely deficient in homing to the LN, and to a lesser extent the spleen (Fig. 2C). To confirm that the homing defect is not due to differential CD62L or CCR7 expression, we quantified the surface phenotype of control eGFP and eGFP-Orai1-E106A transfected human T cells. eGFP-Orai1-E106A⁺ human T cells maintained CD62L expression at marginally lower levels than the control population (Fig. 2D). CCR7 expression was unchanged in both populations (Fig. 2E).

We evaluated whether suppression of Ca^{2+} signaling through Orai1 channels could lead to an accumulation of Orai1-E106A⁺ T cells in the HEV following adoptive transfer. To determine the localization of T cells relative to the HEV, we isolated LNs from NOD.SCID mice following adoptive transfer of equal numbers of control CMTMR-labeled and eGFP-Orai1-E106A-transfected human T cells (Supplemental Fig. 3B). Fixed LNs were sliced from the base of the hilum and stained for peripheral node addressin, a carbohydrate epitope specific for the HEV (40). Both control and eGFP-Orai1-E106A⁺ human T cells were observed in regions that contained HEV (Fig. 3A). Control human T cells (red) were positioned both within and outside of HEV (blue) that perfuse the LN cortex, whereas T cells expressing eGFP-Orai1-E106A (green) were observed predominantly within the HEV (Fig. 3B). Fewer total eGFP-Orai1-E106A⁺ T cells were observed in selected areas containing HEV, compared to control T cells (Supplemental Fig. 3C). Collectively, these findings indicate that human T cells require CRAC channel function for LN homing across the HEV in our xenograft model.

Migration and homing in reconstituted immunocompromised mice

To extend these results on the requirement of CRAC channel function for homing, we performed additional validation studies using NOD.SCID.B2 mice that had been previously reconstituted with human peripheral blood leukocytes (PBL). Reconstitution of immunocompromised mice was achieved by intraperitoneal injection of purified human PBL. Three weeks following PBL injection, LNs and spleens from NOD.SCID.B2 mice increased in size. Mean LN perimeter grew from 0.39 cm to 0.82 cm; mean spleen perimeter increased from 2.0 cm to 3.5 cm (Supplemental Fig. 4A). Hematoxylin and eosin staining of non-reconstituted NOD.SCID.B2 LN slices showed a lack of structure and nuclear density. Cellular density increased following three weeks of reconstitution by human PBL, but cellular density was lower and follicular structure undefined compared to wildtype LNs (Supplemental Fig. 4B). To confirm that human T cells could migrate with characteristic motility behavior in the reconstituted NOD.SCID.B2 LN, $\text{CD}3^{+}$ T cells from the original donor were transferred into the host animal following reconstitution (Supplemental Fig. 1C). Time-lapse two-photon imaging revealed robust T cell migration in the reconstituted LN (Fig. 4A, Supplemental Video 2), where T cells migrated with a mean velocity of $12.8 \pm 0.4 \mu\text{m min}^{-1}$ (Fig. 4B). Human $\text{CD}3^{+}$ T cells migrated away from their starting coordinates, with mean displacement increasing as a square root function of time, typical of a random walk (Fig. 4C, 4D). The average $\text{CD}3^{+}$ step-wise turning angle was 110.9 ± 2.5 degrees (Fig. 4E). Normal representative T cell migration and increased LN cellularity indicated that reconstituted NOD.SCID.B2 mice can also be utilized for analysis of transfected human immune cells.

To validate our finding that human T cells expressing the dominant-negative Orai1 mutant are unable to home to the LN and spleen *in vivo*, we performed a homing study in reconstituted NOD.SCID.B2 mice. Equal numbers of mock-transfected CMTMR-labeled control and Orai1-E106A-transfected human T cells were adoptively transferred into NOD.SCID.B2 mice that had previously been reconstituted with blood from the same donor. Whole-organ flow cytometry revealed that control CMTMR-labeled human T cells homed to the SLO, representing 0.8% and 0.2% of the total cells in the LN and spleen, respectively (Fig. 4F). Human T cells expressing the Orai1-E106A mutant lost their homing capacity to the SLO, representing < 0.1% of the total cellularity in both organs (Fig. 4F). The majority of the cells recovered by flow cytometry were CMTMR⁺ controls (Fig. 4G), demonstrating that eGFP-Orai1-E106A⁺ human cells cannot home to the SLO in the human-reconstituted mouse model.

Homing block in mouse T cells with disrupted CRAC channel function

The results so far point to a requirement for CRAC channel function in the homing of human T cells in acutely and stably engrafted immunocompromised mice. To determine if functional CRAC channels are also required for the homing of mouse T cells into the LN, we engineered MSCV-IRES retroviral vectors containing the variant Thy1.1 gene as a marker for expression, together with either eGFP-Orai1-E106A or a control cyan fluorescent protein (CFP) construct. We then transduced wildtype mouse T cells and examined their Ca^{2+} responses following store depletion by single-cell Ca^{2+} imaging. As expected, Ca^{2+} influx was suppressed in mouse T cells expressing eGFP-Orai1-E106A, relative to control CFP⁺ T cells (Fig. 5A). Using Thy1.1 co-expression and magnetic bead separation to purify cells, we labeled control and eGFP-Orai1-E106A expressing T cells with CMTMR or CFSE, respectively, and evaluated homing following co-transfer into a wildtype recipient (Supplemental Fig. 1D). By flow cytometric analysis of recovered cells, Thy1.1⁻ cells that did not express retroviral constructs were effectively recovered from LN and spleen (Fig. 5B). In addition, Thy1.1⁺CFP⁺ T cells, representing control cells that were successfully transduced, also were able to home to the SLO, representing > 8% of the total cellularity (Fig. 5C, top gate). In contrast, adoptively transferred Thy1.1⁺eGFP-Orai1-E106A⁺ mouse T cells represented < 0.2% of the total cellularity of the LN and spleen (Fig. 5C, bottom gate). We conclude that mouse T cells deficient in CRAC channel function are unable to home to the SLO of syngeneic mice, in agreement with our results using human cells in the xenograft models.

Orai1-E106A expression disrupts CCL21-dependent Ca^{2+} signaling and LFA-1 activation

Because treatment with CCL21 (the chemokine implicated in T cell homing) evokes Ca^{2+} signals in human T cells (25, 26), we hypothesized that CRAC channels mediate this response. To test for CRAC channel activity during the chemokine response we utilized time-lapse flow cytometry to measure Ca^{2+} influx following Tg or CCL21 treatment in untransfected control human T cells and in cells transfected with either eGFP or eGFP-Orai1-E106A (Supplemental Fig. 1E). To achieve this, we used the Ca^{2+} indicator dye fura red, which reports increases in $[\text{Ca}^{2+}]_i$ by a decrease in fluorescence signal. As expected, Tg treatment resulted in a sustained $[\text{Ca}^{2+}]_i$ increase in both untransfected and eGFP⁺ control T cell populations (Fig. 6A). In contrast, cytosolic Ca^{2+} did not change in eGFP-Orai1-E106A⁺ T cells. Recombinant mouse CCL21 stimulation resulted in a rapid and transient rise in $[\text{Ca}^{2+}]_i$, in both control untransfected and eGFP⁺ human T cells. However, human T cells expressing the dominant-negative eGFP-Orai1-E106A construct did not respond to CCL21 (Fig. 6B). Measurements of peak $[\text{Ca}^{2+}]_i$ levels demonstrate that human T cells deficient in CRAC channel function are unable to mobilize Ca^{2+} following Tg or CCL21 treatment (Fig. 6C).

Because CCL21 treatment has been previously shown to induce T cell binding to ICAM-1 (22), we tested whether suppression of CCL21-dependent Ca^{2+} signaling could lead to a defect in migration across a confluent endothelial cell (EC) monolayer *in vitro*. Utilizing a standard chemotaxis assay, migration of control eGFP⁺ or eGFP-Orai1-E106A⁺ human T cells in response to CCL21 was measured across an uncoated polycarbonate transwell. Both T cell populations migrated robustly in response to the chemokine gradient (Fig. 7A), revealing that Orai1 function is not required for chemotaxis in the uncoated transwell. However, eGFP-Orai1-E106A⁺ human T cells were deficient in migrating across transwells coated with ECs independent of the CCL21 concentration (Fig. 7B), suggesting a role for Orai1 in facilitating T cell-EC interactions independent of CCR7. Because chemokine-induced activation of integrins is required for transendothelial migration and lymph node entry (22, 23), we investigated the role of Orai1 in integrin activation following CCL21 treatment (Supplemental Fig. 1F). Flow cytometry revealed that CCL21-induced activation

of LFA-1 integrin was abolished in eGFP-Orai1-E106A⁺ human T cells (Fig. 7C); although VLA-4 β_1 integrin was unaffected (Fig. 7D). Chemokine treatment has been shown to enhance binding of soluble ICAM-1 to leukocytes, demonstrating LFA-1 activation (41). CCL21 treatment enhanced ICAM-1 binding to control T cells, and binding was reduced in eGFP-Orai1-E106A⁺ T cells (Fig. 7E). We conclude that Orai1 is required for CCL21-induced Ca²⁺ signaling in human T cells and subsequent LFA-1 activation, transendothelial migration, and lymph node homing.

Discussion

We show that CRAC channel function is required for T cell homing into SLO. Our results are demonstrated in a combined *in vivo* and *in vitro* assessment of human T cells in mouse xenograft models, as well as in retrovirally transduced mouse T cells in syngeneic recipient mice. By inhibiting native CRAC channels with a dominant-negative Orai1 mutant (E106A), our approach avoids potential compensation in Orai1 knock-out mouse models that retain residual CRAC channel function. Moreover, these results establish a system for live two-photon imaging of labeled or transfected human lymphocytes in an *in vivo* human xenografted mouse environment.

Homing and motility of human lymphocytes in xenografted mice

Using human lymphocytes transferred acutely into immunocompromised mice or into reconstituted human xenografted mice, we describe two-photon imaging of human T and B lymphocytes within intact lymph nodes in a preparation that does not require human fetal tissue. Our methods differ from a recent study which utilized two-photon microscopy to image human T cell migration in mice reconstituted using fetal human blood, liver, and thymus (BLT mice) (42). Both NOD.SCID and NOD.SCID.B2 mice retain peripheral LNs that support engraftment of human lymphocytes. These two strains were chosen because LNs from other immunocompromised mouse strains, including Rag2^{-/-} and NSG, are even more atrophied (43, 44), rendering them unsuitable for imaging. NOD.SCID mice require depletion of resident NK cells before transfer of human lymphocytes and LNs remain small following engraftment, although imaging was possible. Conversely, NOD.SCID.B2 mice readily support human xenografts, allowing for expansion of lymphocyte populations and stable engraftment of human PBLs. Following reconstitution, LNs are enlarged and easily employed for tracking individual labeled cells from the same blood donor by two-photon microscopy.

Our results demonstrate that adoptive transfer, both acutely and into reconstituted SCID mouse models, enables quantitative imaging and analysis of human cells. Human T cells homed into and actively migrated through the atrophied mouse host LNs of NOD.SCID mice with velocities that were somewhat slower than mouse T cells in the same environment (9.3 ± 0.4 vs. $10.9 \pm 0.2 \mu\text{m min}^{-1}$, respectively), similar to velocities reported for the BLT mouse model (42). Compared to the acutely transferred model, human T cells transferred into reconstituted mice migrated with faster mean velocity ($12.8 \pm 0.4 \mu\text{m min}^{-1}$), closely similar to wildtype mouse T cells in the LN (27). Human T and B cell relative velocities mirrored the migration of mouse lymphocytes; both human and mouse T cells migrate more rapidly than CD19⁺ B cells in the xenograft environment (Fig. 1), as originally observed for mouse T and B cells in mouse lymph node (39). Displacement analysis confirmed that, like mouse B cells, human B cells migrate with lower velocities and motility coefficients than T cells, reflecting slower migration. Our results suggest that more rapid migration is an intrinsic characteristic of T cells.

CRAC channel activity required for homing

Our results utilized the dominant-negative Orai1-E106A mutant to suppress CRAC channel function in mouse and human T cells and thereby elucidate mechanisms by which these ion channels regulate T cell function. Orai1-E106A has been used previously to determine the requirements for Orai1 clustering at the immunological synapse (33), to identify STIM1-Orai1 interacting domains (45), to determine regulation of voltage-gated Ca^{2+} channels by STIM1 (46), to reveal mechanisms for protection against apoptotic signaling through CD95 (47), and to demonstrate Ca^{2+} release from secretory granules (48). In Orai1-deficient mice, Ca^{2+} entry is not fully abolished in T cells (17, 18). Moreover, whereas human patients with the homozygous Orai1-R91W mutation do not have functional CRAC channels (7), knock-in mice with the analogous mouse Orai1-R93W mutation maintain residual Ca^{2+} influx, and show normal LN cellularity despite impaired T cell function. However, upon adoptive transfer into a Rag2^{-/-} mouse, Orai1-R93W CD4⁺ T cells were significantly impaired in homing to the mesenteric LN, compared to wildtype T cells (49). In comparison to these knock-in and knock-out mouse models, our use of Orai1-E106A expression specifically and completely suppresses CRAC channel function in human and mouse T cells, which we demonstrate to result in a severe homing defect in both the xenograft or wildtype mouse environment (Figs. 2, 4, 5).

We further show that transendothelial migration and homing of lymphocytes to lymph nodes requires Ca^{2+} influx through Orai1 channels. During homing, T cells must adhere to endothelial cells and then extravasate from the HEV to the LN paracortex. Consistent with a role of Ca^{2+} influx, our results demonstrate that Orai1 assists in LFA-1 ($\alpha_1\beta_2$ integrin) activation by providing the initial Ca^{2+} signal in response to CCL21 treatment. We previously showed that inhibition of Kv1.3 channels, which are required for sustained Ca^{2+} signaling in lymphocytes (12), disrupts VLA-4 ($\alpha_4\beta_1$ integrin) activation in effector memory T cells and inhibits their migration in inflamed tissues (50). Our results do not fully account for where eGFP-Orai1-E106A⁺ T cells reside following transfer. Other studies also support a requirement for Ca^{2+} signaling in T cell migration. T cell-specific deletion of the STIM proteins that activate Orai1 Ca^{2+} channels abolishes chemokine-induced Ca^{2+} influx and diminishes chemotaxis towards chemokine gradients (51). Orai1 has also been proposed to mediate migrational guidance in response to high-affinity LFA-1-ICAM interactions following shear stress in neutrophils (52) and in chemotaxis of platelets (53). Moreover, CCR7 signaling enhances overall lymphocyte motility (chemokinesis) in the LN following homing (54-57). Thus, CCR7 signaling and the resulting CRAC channel activation mediated by STIM1-Orai1 interaction may modulate both homing and chemokinesis by enhancing intercellular adhesion. Our findings extend the scope of immune system functions controlled by Orai1 to include homing, integrin activation, and transendothelial migration.

Supplementary Material

Refer to Web version on PubMed Central for supplementary material.

Acknowledgments

We thank Drs. Lurette Forrest and Olga Safrina for expert assistance and Dr. Aubin Penna for design and purification of constructs. We acknowledge the UCI Optical Biology Core, and Vanessa Scarfone of the flow cytometry core supported by the California Institute for Regenerative Medicine (CIRM).

This project was supported by NIH Grants NS-14609 and GM-41514 to MDC, GM-48071 to IP, NIH Immunology Research Training Program Grant T32-AI-060573 to MG, and in part by the American Heart Association Scientist Development Grant (0630117N to YY). Human blood was prepared using support from the National Center for Research Resources and the National Center for Advancing Translational Sciences, Grant NIH grant UL1 TR000153.

Abbreviations used in this paper

B2	beta-2 microglobulin
CFP	cyan fluorescent protein
CRAC	Ca ²⁺ release-activated Ca ²⁺ channel
[Ca²⁺]_i	intracellular calcium concentration
EC	endothelial cell
eGFP	enhanced green fluorescent protein
ER	endoplasmic reticulum
HEV	high endothelial venules
LFA-1	integrin lymphocyte function-associated antigen-1
LN	lymph node
NOD.SCID	non-obese diabetic severe combined immunodeficient mouse
SLO	secondary lymphoid organs
STIM	stromal interacting molecule
Tg	thapsigargin
VLA-4	integrin very late antigen-4

References

1. Feske S. Calcium signalling in lymphocyte activation and disease. *Nat. Rev. Immunol.* 2007; 7:690–702. [PubMed: 17703229]
2. Negulescu PA, Shastri N, Cahalan MD. Intracellular calcium dependence of gene expression in single T lymphocytes. *Proc. Natl. Acad. Sci. USA.* 1994; 91:2873–2877. [PubMed: 8146203]
3. Negulescu PA, Krasieva TB, Khan A, Kerschbaum HH, Cahalan MD. Polarity of T cell shape, motility, and sensitivity to antigen. *Immunity.* 1996; 4:421–430. [PubMed: 8630728]
4. Yeromin AV, Zhang SL, Jiang W, Yu Y, Safrina O, Cahalan MD. Molecular identification of the CRAC channel by altered ion selectivity in a mutant of Orai. *Nature.* 2006; 443:226–229. [PubMed: 16921385]
5. Prakriya M, Feske S, Gwack Y, Srikanth S, Rao A, Hogan PG. Orai1 is an essential pore subunit of the CRAC channel. *Nature.* 2006; 443:230–233. [PubMed: 16921383]
6. Vig M, Beck A, Billingsley JM, Lis A, Parvez S, Peinelt C, Koomoa DL, Soboloff J, Gill DL, Fleig A, Kinet JP, Penner R. CRACM1 multimers form the ion-selective pore of the CRAC channel. *Curr. Biol.* 2006; 16:2073–2079. [PubMed: 16978865]
7. Feske S, Gwack Y, Prakriya M, Srikanth S, Puppel SH, Tanasa B, Hogan PG, Lewis RS, Daly M, Rao A. A mutation in Orai1 causes immune deficiency by abrogating CRAC channel function. *Nature.* 2006; 441:179–185. [PubMed: 16582901]
8. Vig M, Peinelt C, Beck A, Koomoa DL, Rabah D, Koblan-Huberson M, Kraft S, Turner H, Fleig A, Penner R, Kinet JP. CRACM1 is a plasma membrane protein essential for store-operated Ca²⁺ entry. *Science.* 2006; 312:1220–1223. [PubMed: 16645049]
9. Zhang SL, Yeromin AV, Zhang XH, Yu Y, Safrina O, Penna A, Roos J, Stauderman KA, Cahalan MD. Genome-wide RNAi screen of Ca²⁺ influx identifies genes that regulate Ca²⁺ release-activated Ca²⁺ channel activity. *Proc. Natl. Acad. Sci. USA.* 2006; 103:9357–9362. [PubMed: 16751269]
10. Cahalan MD. STIMulating store-operated Ca²⁺ entry. *Nat. Cell Biol.* 2009; 11:669–677. [PubMed: 19488056]

11. Hogan PG, Lewis RS, Rao A. Molecular basis of calcium signaling in lymphocytes: STIM and ORAI. *Annu. Rev. Immunol.* 2010; 28:491–533. [PubMed: 20307213]
12. Cahalan MD, Chandy KG. The functional network of ion channels in T lymphocytes. *Immunol. Rev.* 2009; 231:59–87. [PubMed: 19754890]
13. Picard C, McCarl CA, Papolos A, Khalil S, Luthy K, Hivroz C, LeDeist F, Rieux-Laucat F, Rechavi G, Rao A, Fischer A, Feske S. STIM1 mutation associated with a syndrome of immunodeficiency and autoimmunity. *New England Journal of Medicine.* 2009; 360:1971–1980. [PubMed: 19420366]
14. Fuchs S, Rensing-Ehl A, Speckmann C, Bengsch B, Schmitt-Graeff A, Bondzio I, Maul-Pavicic A, Bass T, Vraetz T, Strahm B, Ankermann T, Benson M, Caliebe A, Folster-Holst R, Kaiser P, Thimme R, Schamel WW, Schwarz K, Feske S, Ehl S. Antiviral and regulatory T cell immunity in a patient with stromal interaction molecule 1 deficiency. *J. Immunol.* 2012; 188:1523–1533. [PubMed: 22190180]
15. Byun M, Abhyankar A, Lelarge V, Plancoulaine S, Palanduz A, Telhan L, Boisson B, Picard C, Dewell S, Zhao C, Jouanguy E, Feske S, Abel L, Casanova JL. Whole-exome sequencing-based discovery of STIM1 deficiency in a child with fatal classic Kaposi sarcoma. *J. Exp. Med.* 2010; 207:2307–2312. [PubMed: 20876309]
16. Feske S, Picard C, Fischer A. Immunodeficiency due to mutations in ORAI1 and STIM1. *Clin. Immunol.* 2010; 135:169–182. [PubMed: 20189884]
17. Vig M, DeHaven WI, Bird GS, Billingsley JM, Wang H, Rao PE, Hutchings AB, Jouvin MH, Putney JW, Kinet JP. Defective mast cell effector functions in mice lacking the CRACM1 pore subunit of store-operated calcium release-activated calcium channels. *Nat. Immunol.* 2008; 9:89–96. [PubMed: 18059270]
18. Gwack Y, Srikanth S, Oh-Hora M, Hogan PG, Lamperti ED, Yamashita M, Gelinis C, Neems DS, Sasaki Y, Feske S, Prakriya M, Rajewsky K, Rao A. Hair loss and defective T- and B-cell function in mice lacking ORAI1. *Mol. Cell. Biol.* 2008; 28:5209–5222. [PubMed: 18591248]
19. Salmi M, Jalkanen S. Cell-surface enzymes in control of leukocyte trafficking. *Nat. Rev. Immunol.* 2005; 5:760–771. [PubMed: 16200079]
20. Ley K, Laudanna C, Cybulsky MI, Nourshargh S. Getting to the site of inflammation: the leukocyte adhesion cascade updated. *Nat. Rev. Immunol.* 2007; 7:678–689. [PubMed: 17717539]
21. Vestweber D. Molecular mechanisms that control leukocyte extravasation through endothelial cell contacts. *Ernst Schering Foundation Symposium Proceedings.* 2007:151–167. [PubMed: 18512285]
22. Gunn MD, Tangemann K, Tam C, Cyster JG, Rosen SD, Williams LT. A chemokine expressed in lymphoid high endothelial venules promotes the adhesion and chemotaxis of naive T lymphocytes. *Proc. Natl. Acad. Sci. USA.* 1998; 95:258–263. [PubMed: 9419363]
23. Forster R, Davalos-Misslitz AC, Rot A. CCR7 and its ligands: balancing immunity and tolerance. *Nat. Rev. Immunol.* 2008; 8:362–371. [PubMed: 18379575]
24. Stewart MP, McDowall A, Hogg N. LFA-1-mediated adhesion is regulated by cytoskeletal restraint and by a Ca²⁺-dependent protease, calpain. *J. Cell Biol.* 1998; 140:699–707. [PubMed: 9456328]
25. Nagira M, Imai T, Hieshima K, Kusuda J, Ridanpaa M, Takagi S, Nishimura M, Kakizaki M, Nomiyama H, Yoshie O. Molecular cloning of a novel human CC chemokine secondary lymphoid-tissue chemokine that is a potent chemoattractant for lymphocytes and mapped to chromosome 9p13. *J. Biol. Chem.* 1997; 272:19518–19524. [PubMed: 9235955]
26. Randolph DA, Huang G, Carruthers CJ, Bromley LE, Chaplin DD. The role of CCR7 in TH1 and TH2 cell localization and delivery of B cell help in vivo. *Science.* 1999; 286:2159–2162. [PubMed: 10591648]
27. Cahalan MD, Parker I. Choreography of cell motility and interaction dynamics imaged by two-photon microscopy in lymphoid organs. *Annu. Rev. Immunol.* 2008; 26:585–626. [PubMed: 18173372]
28. Shultz LD, Schweitzer PA, Christianson SW, Gott B, Schweitzer IB, Tennent B, McKenna S, Mobraaten L, Rajan TV, Greiner DL, et al. Multiple defects in innate and adaptive immunologic function in NOD/LtSz-scid mice. *J. Immunol.* 1995; 154:180–191. [PubMed: 7995938]

29. Ito M, Hiramatsu H, Kobayashi K, Suzue K, Kawahata M, Hioki K, Ueyama Y, Koyanagi Y, Sugamura K, Tsuji K, Heike T, Nakahata T. NOD/SCID/gamma(c)(null) mouse: an excellent recipient mouse model for engraftment of human cells. *Blood*. 2002; 100:3175–3182. [PubMed: 12384415]
30. Mosier DE, Gulizia RJ, Baird SM, Wilson DB. Transfer of a functional human immune system to mice with severe combined immunodeficiency. *Nature*. 1988; 335:256–259. [PubMed: 2970594]
31. Shultz LD, Ishikawa F, Greiner DL. Humanized mice in translational biomedical research. *Nat. Rev. Immunol.* 2007; 7:118–130. [PubMed: 17259968]
32. Christianson SW, Greiner DL, Hesselton RA, Leif JH, Wagar EJ, Schweitzer IB, Rajan TV, Gott B, Roopenian DC, Shultz LD. Enhanced human CD4⁺ T cell engraftment in beta2-microglobulin-deficient NOD-scid mice. *J. Immunol.* 1997; 158:3578–3586. [PubMed: 9103418]
33. Lioudyno MI, Kozak JA, Penna A, Safrina O, Zhang SL, Sen D, Roos J, Stauderman KA, Cahalan MD. Orai1 and STIM1 move to the immunological synapse and are up-regulated during T cell activation. *Proc. Natl. Acad. Sci. USA.* 2008; 105:2011–2016. [PubMed: 18250319]
34. Newton RH, Leverrier S, Srikanth S, Gwack Y, Cahalan MD, Walsh CM. Protein kinase D orchestrates the activation of DRAK2 in response to TCR-induced Ca²⁺ influx and mitochondrial reactive oxygen generation. *J. Immunol.* 2011; 186:940–950. [PubMed: 21148796]
35. Matheu MP, Su Y, Greenberg ML, Blanc CA, Parker I, Scott DW, Cahalan MD. Toll-like receptor 4-activated B cells out-compete Toll-like receptor 9-activated B cells to establish peripheral immunological tolerance. *Proc. Natl. Acad. Sci. USA.* 2012; 109:E1258–1266. [PubMed: 22511718]
36. Zhang SL, Kozak JA, Jiang W, Yeromin AV, Chen J, Yu Y, Penna A, Shen W, Chi V, Cahalan MD. Store-dependent and -independent modes regulating Ca²⁺ release-activated Ca²⁺ channel activity of human Orai1 and Orai3. *J. Biol. Chem.* 2008; 283:17662–17671. [PubMed: 18420579]
37. Lev-Ram V, Miyakawa H, Lasser-Ross N, Ross WN. Calcium transients in cerebellar Purkinje neurons evoked by intracellular stimulation. *J. Neurophysiol.* 1992; 68:1167–1177. [PubMed: 1432076]
38. Newman AC, Nakatsu MN, Chou W, Gershon PD, Hughes CC. The requirement for fibroblasts in angiogenesis: fibroblast-derived matrix proteins are essential for endothelial cell lumen formation. *Mol. Biol. Cell.* 2011; 22:3791–3800. [PubMed: 21865599]
39. Miller MJ, Wei SH, Parker I, Cahalan MD. Two-photon imaging of lymphocyte motility and antigen response in intact lymph node. *Science.* 2002; 296:1869–1873. [PubMed: 12016203]
40. Streeter PR, Rouse BT, Butcher EC. Immunohistologic and functional characterization of a vascular addressin involved in lymphocyte homing into peripheral lymph nodes. *J. Cell Biol.* 1988; 107:1853–1862. [PubMed: 2460470]
41. Flach H, Rosenbaum M, Duchniewicz M, Kim S, Zhang SL, Cahalan MD, Mittler G, Grosschedl R. Mzb1 protein regulates calcium homeostasis, antibody secretion, and integrin activation in innate-like B cells. *Immunity.* 2010; 33:723–735. [PubMed: 21093319]
42. Murooka TT, Deruaz M, Marangoni F, Vrbanac VD, Seung E, von Andrian UH, Tager AM, Luster AD, Mempel TR. HIV-infected T cells are migratory vehicles for viral dissemination. *Nature.* 2012; 490:283–287. [PubMed: 22854780]
43. Shinkai Y, Rathbun G, Lam KP, Oltz EM, Stewart V, Mendelsohn M, Charron J, Datta M, Young F, Stall AM, et al. RAG-2-deficient mice lack mature lymphocytes owing to inability to initiate V(D)J rearrangement. *Cell.* 1992; 68:855–867. [PubMed: 1547487]
44. Shultz LD, Lyons BL, Burzenski LM, Gott B, Chen X, Chaleff S, Kotb M, Gillies SD, King M, Mangada J, Greiner DL, Handgretinger R. Human lymphoid and myeloid cell development in NOD/LtSz-scid IL2R gamma null mice engrafted with mobilized human hemopoietic stem cells. *J. Immunol.* 2005; 174:6477–6489. [PubMed: 15879151]
45. Park CY, Hoover PJ, Mullins FM, Bachhawat P, Covington ED, Raunser S, Walz T, Garcia KC, Dolmetsch RE, Lewis RS. STIM1 clusters and activates CRAC channels via direct binding of a cytosolic domain to Orai1. *Cell.* 2009; 136:876–890. [PubMed: 19249086]
46. Wang Y, Deng X, Mancarella S, Hendron E, Eguchi S, Soboloff J, Tang XD, Gill DL. The calcium store sensor, STIM1, reciprocally controls Orai and CaV1.2 channels. *Science.* 2010; 330:105–109. [PubMed: 20929813]

47. Khadra N, Bresson-Bepoldin L, Penna A, Chaigne-Delalande B, Segui B, Levade T, Vacher AM, Reiffers J, Ducret T, Moreau JF, Cahalan MD, Vacher P, Legembre P. CD95 triggers Orai1-mediated localized Ca^{2+} entry, regulates recruitment of protein kinase C (PKC) β_2 , and prevents death-inducing signaling complex formation. *Proc. Natl. Acad. Sci. USA.* 2011; 108:19072–19077. [PubMed: 22065776]
48. Dickson EJ, Duman JG, Moody MW, Chen L, Hille B. Orai-STIM-mediated Ca^{2+} release from secretory granules revealed by a targeted Ca^{2+} and pH probe. *Proc. Natl. Acad. Sci. USA.* 2012; 109:E3539–3548. [PubMed: 23184982]
49. McCarl CA, Khalil S, Ma J, Oh-hora M, Yamashita M, Roether J, Kawasaki T, Jairaman A, Sasaki Y, Prakriya M, Feske S. Store-operated Ca^{2+} entry through ORAI1 is critical for T cell-mediated autoimmunity and allograft rejection. *J. Immunol.* 2010; 185:5845–5858. [PubMed: 20956344]
50. Matheu MP, Beeton C, Garcia A, Chi V, Rangaraju S, Safrina O, Monaghan K, Uemura MI, Li D, Pal S, de la Maza LM, Monuki E, Flugel A, Pennington MW, Parker I, Chandy KG, Cahalan MD. Imaging of effector memory T cells during a delayed-type hypersensitivity reaction and suppression by Kv1.3 channel block. *Immunity.* 2008; 29:602–614. [PubMed: 18835197]
51. Ma J, McCarl CA, Khalil S, Luthy K, Feske S. T-cell-specific deletion of STIM1 and STIM2 protects mice from EAE by impairing the effector functions of Th1 and Th17 cells. *Eur. J. Immunol.* 2010; 40:3028–3042. [PubMed: 21061435]
52. Dixit N, Yamayoshi I, Nazarian A, Simon SI. Migrational guidance of neutrophils is mechanotransduced via high-affinity LFA-1 and calcium flux. *J. Immunol.* 2011; 187:472–481. [PubMed: 21632714]
53. Schmidt EM, Munzer P, Borst O, Kraemer BF, Schmid E, Urban B, Lindemann S, Ruth P, Gawaz M, Lang F. Ion channels in the regulation of platelet migration. *Biochem. Biophys. Res. Commun.* 2011; 415:54–60. [PubMed: 22005466]
54. Huang JH, Cardenas-Navia LI, Caldwell CC, Plumb TJ, Radu CG, Rocha PN, Wilder T, Bromberg JS, Cronstein BN, Sitkovsky M, Dewhirst MW, Dustin ML. Requirements for T lymphocyte migration in explanted lymph nodes. *J. Immunol.* 2007; 178:7747–7755. [PubMed: 17548612]
55. Worbs T, Mempel TR, Bolter J, von Andrian UH, Forster R. CCR7 ligands stimulate the intranodal motility of T lymphocytes in vivo. *J. Exp. Med.* 2007; 204:489–495. [PubMed: 17325198]
56. Asperti-Boursin F, Real E, Bismuth G, Trautmann A, Donnadieu E. CCR7 ligands control basal T cell motility within lymph node slices in a phosphoinositide 3-kinase-independent manner. *J. Exp. Med.* 2007; 204:1167–1179. [PubMed: 17485513]
57. Okada T, Cyster JG. CC chemokine receptor 7 contributes to Gi-dependent T cell motility in the lymph node. *J. Immunol.* 2007; 178:2973–2978. [PubMed: 17312142]

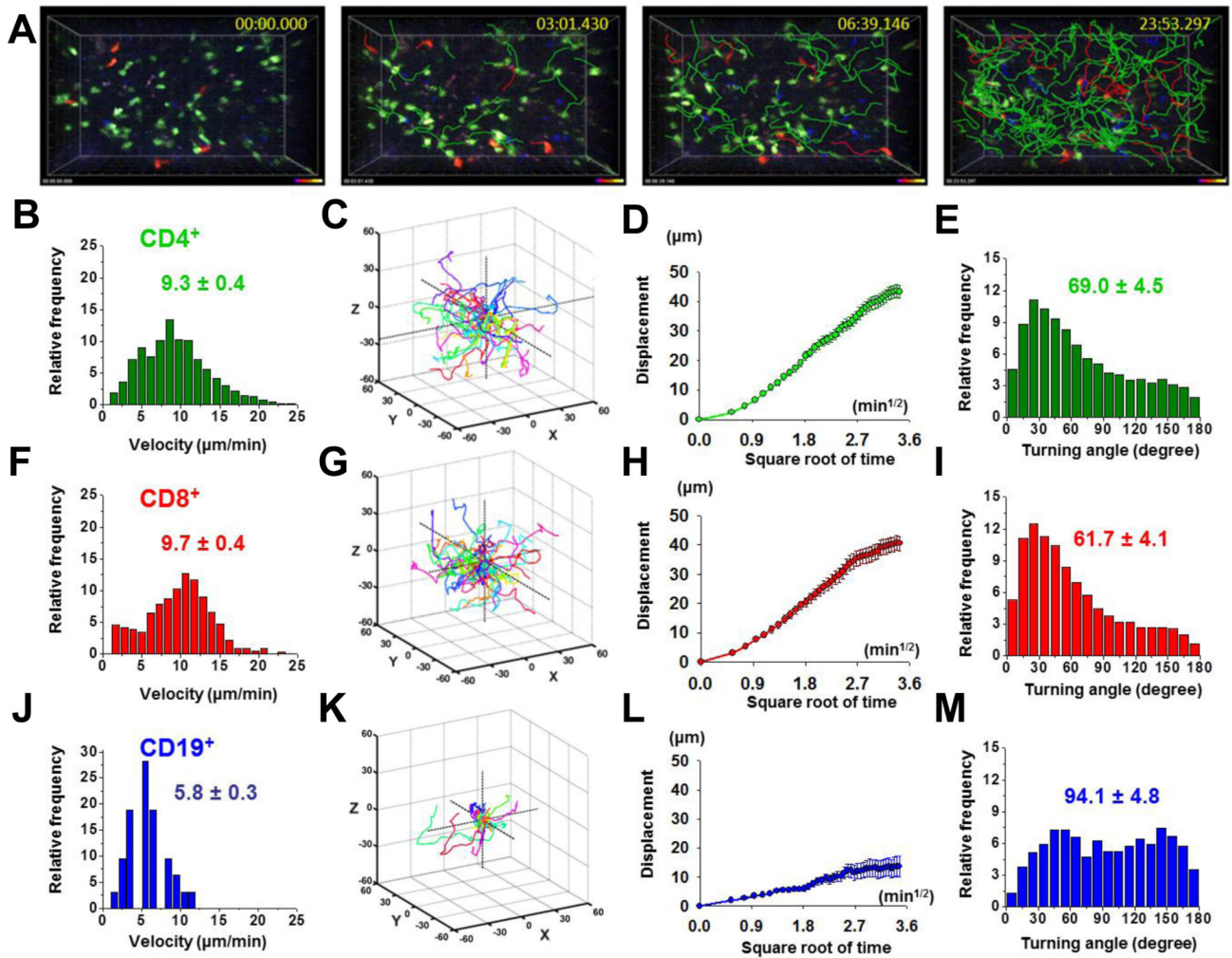


FIGURE 1.

Human lymphocytes actively migrate through explanted lymph nodes of NOD.SCID mice. *A*, Time lapse images of migrating human lymphocytes, showing human CD4⁺ T cells (green), CD8⁺ T cells (red), and CD19⁺ B cells (blue). Correspondingly colored cell tracks depict cell movements over the indicated time periods. *B*, Distribution of mean cellular velocities of 108 human CD4⁺ T cells. Overall mean \pm SEM indicated. *C*, Three-dimensional tracks of 20 human CD4⁺ T cells monitored over 10 min, normalized to their starting coordinates. *D*, Mean displacement of the 20 T cells as a function of the square root of time. *E*, Turning Angles between individual CD4⁺ T cell steps over 10 min intervals, shown with mean angle \pm SEM. *F*, Mean cellular velocities of human CD8⁺ T cells, 118 individual cell tracks. *G*, Three-dimensional tracks of 20 human CD8⁺ T cells monitored throughout ten-minute intervals. *H*, Mean displacement of the 20 T cells. *I*, Distribution of turning angles between CD8⁺ T cell steps. *J*, Mean cellular velocities of human CD19⁺ B cells, 98 individual cell tracks. *K*, Three-dimensional tracks of 10 human CD19⁺ B cells monitored throughout 10 min intervals. *L*, Mean displacement of the 10 B cells. *M*, Distribution of turning angles between CD19⁺ B cell steps.

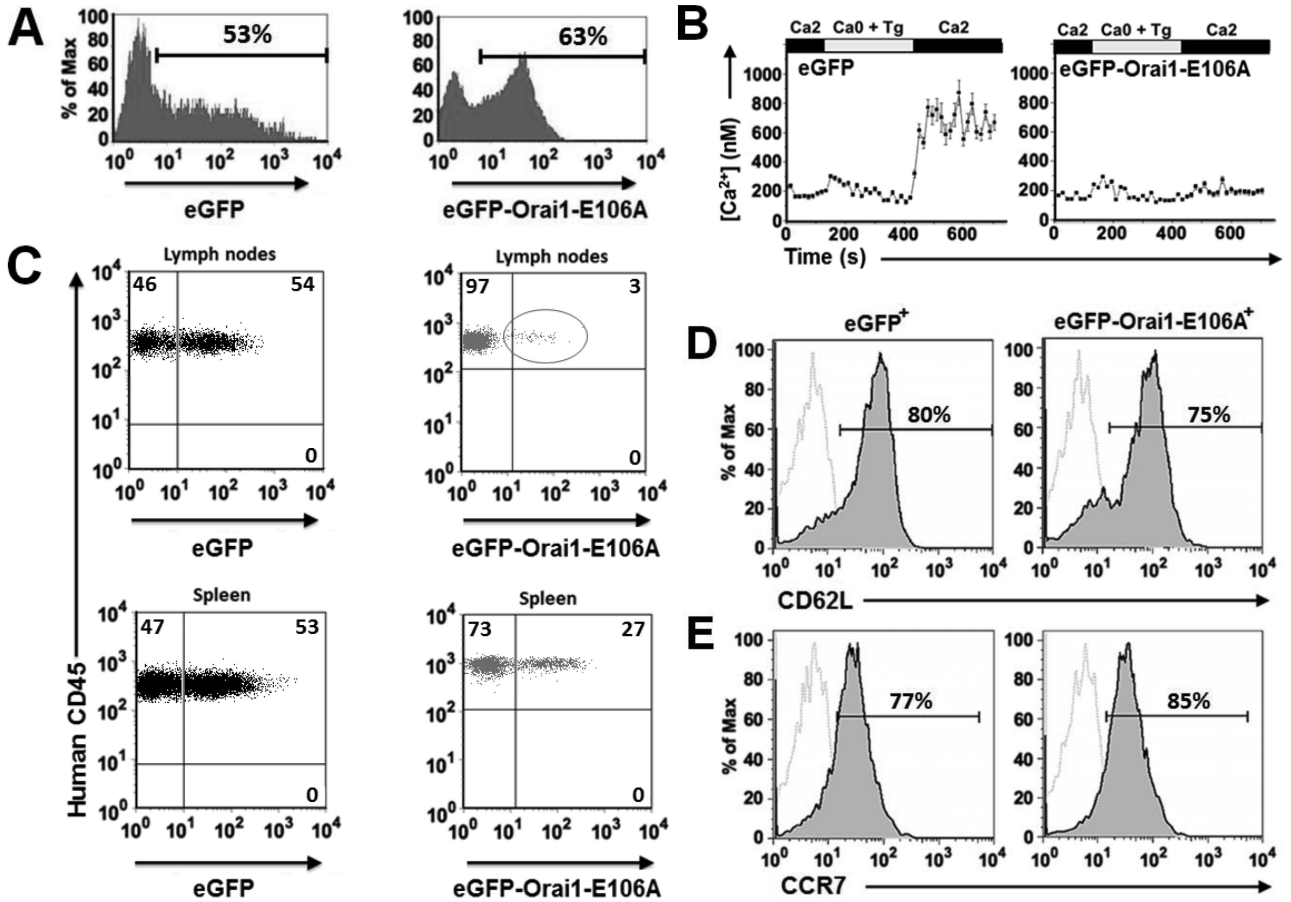


FIGURE 2. Human T cells expressing Orai1-E106A cannot home into the secondary lymphoid organs of NOD.SCID mice. *A*, Expression of eGFP and eGFP-Orai1-E106A in human T cells 24 hr following transfection. *B*, Averaged Tg-dependent influx of Ca²⁺ in human T cells expressing eGFP or eGFP-Orai1-E106A. Data are representative of three different experiments. *C*, Human lymphocyte homing capacity in NOD.SCID mouse LN and spleen 18 hr after adoptive transfer. Percentage of human cells expressing eGFP or eGFP-Orai1-E106A in SLO determined by flow cytometry. *D*, Surface expression of CD62L on eGFP⁺ (left) and eGFP-Orai1-E106A⁺ human T cells (right), 18 hr post-transfection. Isotype control staining represented in dotted gray lines. *E*, Surface expression of CCR7 on eGFP⁺ (left) and eGFP-Orai1-E106A⁺ human T cells (right), 18 hr post-transfection. FACS plots are representative of three separate experiments.

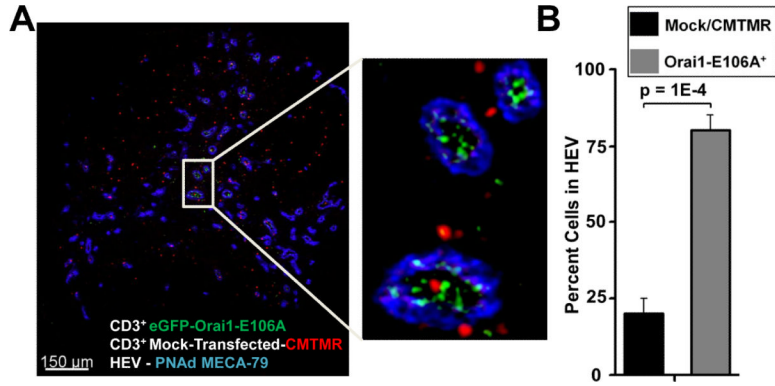


FIGURE 3. Human T cells expressing Orai1-E106A remain localized to the HEV. *A*, Localization of human CD3⁺ T cells in the LN of a NOD.SCID mouse. This image shows CMTMR-labeled control (red) or eGFP-Orai1-E106A-transfected (green) human CD3⁺ T cells in a LN slice from a NOD.SCID mouse. HEVs were labeled with anti- peripheral node addressin (PNAd) antibody MECA-79. The inset shows labeled human cells localized in the HEV and cortex. *B*, The percentage of human T cells found within the HEV.

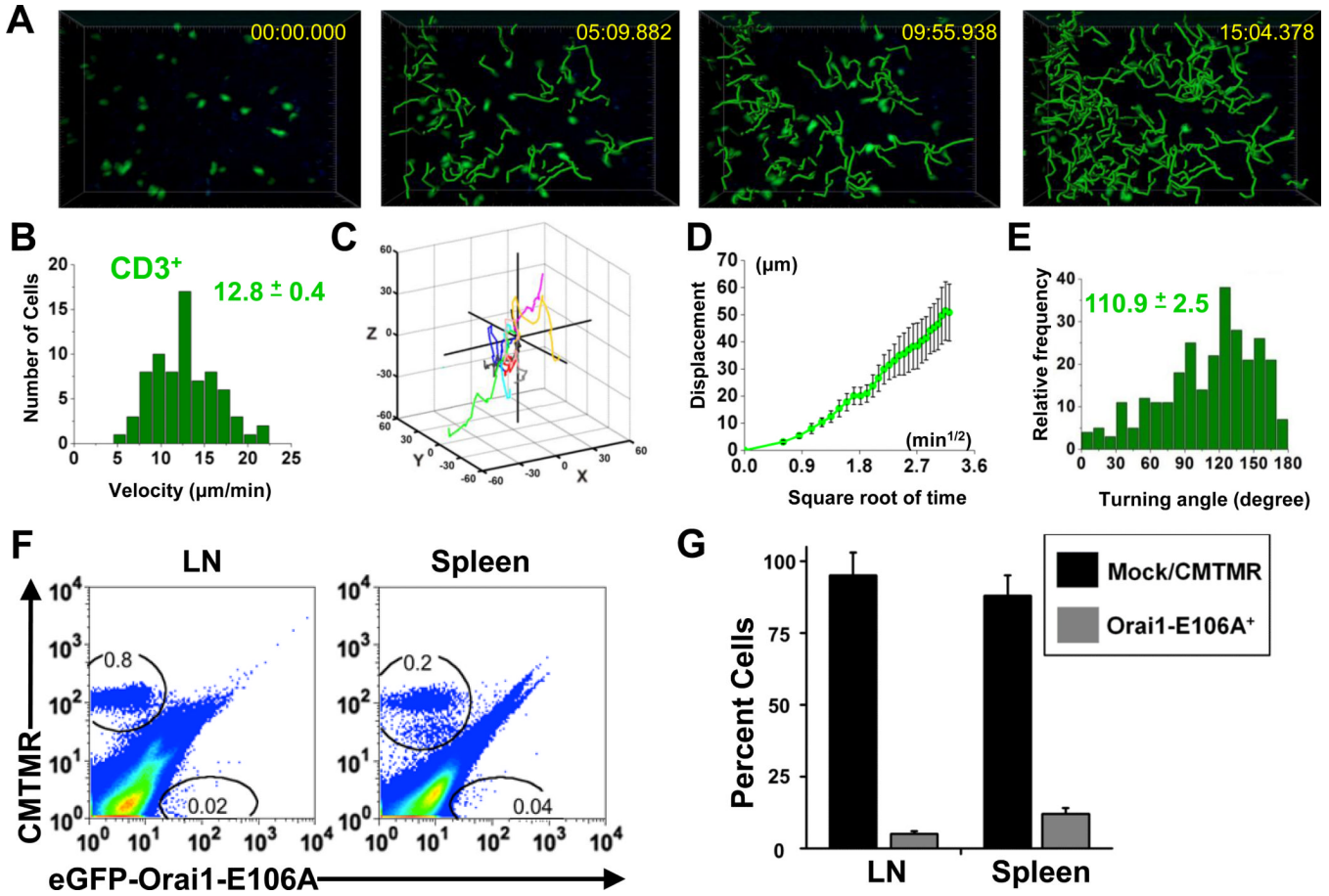
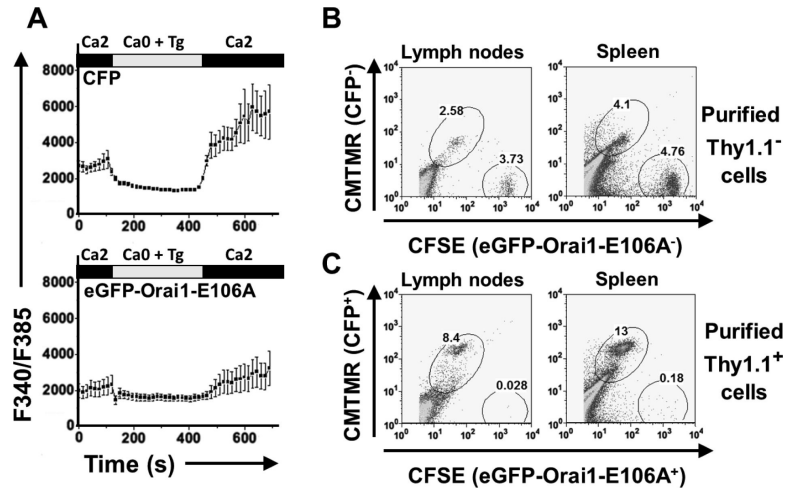


FIGURE 4.

Human T cell motility and homing in the SLO of reconstituted NOD.SCID.B2 mice. *A*, Time lapse two-photon image in an explanted reconstituted NOD.SCID.B2 lymph node, showing transferred human CD3⁺ T cells labeled with CMTMR (pseudocolored green). Panels depict cell positions at the times indicated, together with superimposed tracks depicting progressive cellular migration since the beginning of the record. *B*, Mean cellular velocities of human CD3⁺ T cells shown with the mean \pm SEM, 74 individual cell tracks. *C*, Three-dimensional tracks of 10 human CD3⁺ T cells monitored throughout over 10 min intervals, normalized to starting coordinates. *D*, Mean displacement of the 10 T cells as a square root function of time. *E*, Distribution of turning angles between individual CD3⁺ T cell steps over 10 min intervals shown with mean turning angle \pm SEM. *F*, Homing of control CMTMR⁺ or eGFP-Orai1-E106A⁺ human CD3⁺ T cells in the reconstituted NOD.SCID.B2 mouse. T cell gates are drawn as indicated. *G*, Percent \pm SEM of recovered cells following adoptive transfer, detected by flow cytometry (three individual donors). $p < 0.001$.

**FIGURE 5.**

Mouse T cells expressing Orai1-E106A cannot take up Ca²⁺ or home to the SLO of wildtype syngeneic mice. *A*, Fura-2 fluorescence ratios in transduced mouse CD3⁺ T cells loaded with fura-2. *B*, Homing of control mouse T cells following transduction. Successfully transduced cells (Thy1.1⁺) were purified via positive selection. Unbound mouse T cells (Thy1.1⁻) transduced with the CFP vector were labeled with CMTMR and Thy1.1⁻ cells transduced with the eGFP-Orai1-E106A vector were labeled with CFSE and adoptively transferred. Whole organs were analyzed with T cell gates are drawn as indicated. *C*, Homing of positively isolated (Thy1.1⁺) mouse T cells. Cells were labeled: CFP⁺ with CMTMR and eGFP-Orai1-E106A⁺ with CFSE.

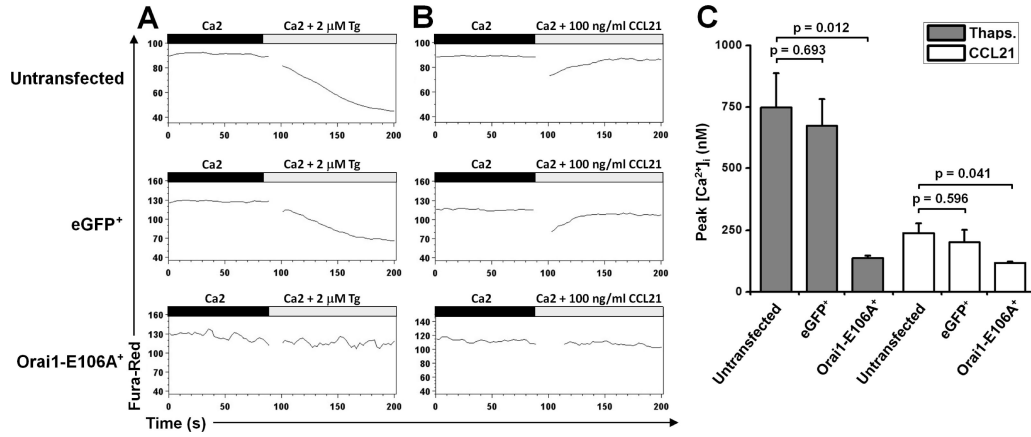


FIGURE 6. Inhibition of Ca²⁺ signals evoked by Tg or CCL21 treatment in human T cells expressing Orai1-E106A. *A*, Flow cytometry analysis, using the FlowJo Kinetics tool, of human T cells loaded with fura red. After 90 sec to establish a baseline, cells were treated with 2 μM Tg. Mean fluorescence changes (lower fluorescence = higher (Ca²⁺)_i) are shown in untransfected human T cells (top), eGFP⁺ human T cells (middle), and eGFP-Orai1-E106A⁺ human T cells (bottom). *B*, Fluorescence changes in untransfected human T cells (top), eGFP⁺ human T cells (middle), and eGFP-Orai1-E106A⁺ human T cells (bottom) following addition of 100 ng/ml recombinant mouse CCL21. Data are from one donor and are representative of three donors. *C*, Mean peak [Ca²⁺]_i signals evoked by Tg and CCL21 in control and eGFP-Orai1-E106A⁺ human T cells.

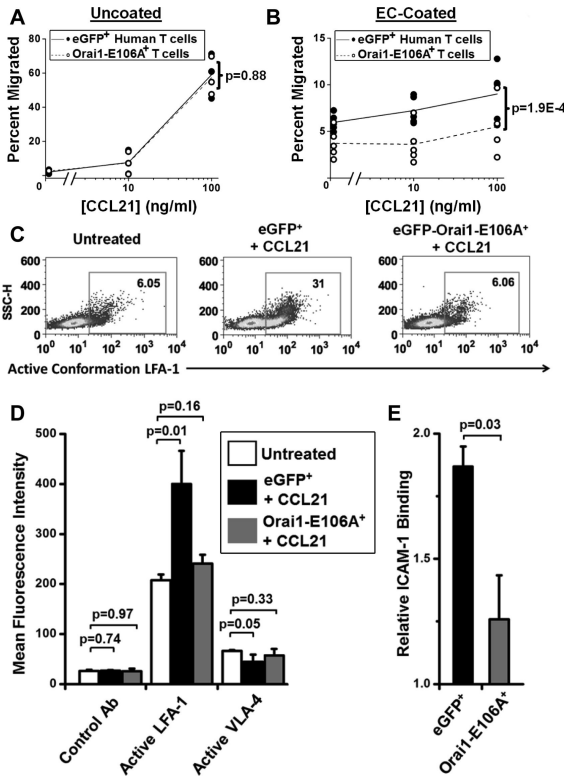


FIGURE 7. Orai1 function is required for transendothelial migration and LFA-1 activation. *A*, T cell migration measured in an uncoated transwell assay in response to different concentrations of recombinant mouse CCL21. Results are expressed as the percentage of cells of each subtype that migrated to the lower chamber of a transwell filter. In each panel, square symbols represent individual experiments showing control eGFP⁺ T cell migration and circles represent eGFP-Orai1-E106A⁺ T cells. n = 3 separate donors. *B*, T cell migration measured in EC-coated transwells in response to CCL21. n = 5. Statistics were determined with two-way ANCOVA. *C*, Representative flow cytometry histograms of active conformation LFA-1 following CCL21 treatment. Secondary control Ab represented in unfilled grey. *D*, Mean fluorescence intensities of human T cells from (*C*) stained with conformation-specific LFA-1 or VLA-4 antibodies. n = 3. *E*, Soluble ICAM-1/Fc binding to human T cells transfected with eGFP or eGFP-Orai1-E106A and treated with CCL21, normalized to ICAM-1/Fc binding to untreated controls. n = 3.